Journal of Thermal Analysis and Calorimetry, Vol. 65 (2001) 185–195

SHORT-RANGE-ORDERING KINETICS OF Cu–5 AT.% Zn INFLUENCED BY SOLUTE–VACANCY COMPLEXES AND COLD ROLLING

A. Varschavsky[*] *and E. Donoso*

Universidad de Chile, Facultad de Ciencias Físicas y Matemáticas, Instituto de Investigaciones y Ensayes de Materiales, IDIEM, Casilla 1420, Santiago, Chile

(Received September 2, 2000; in revised form January 18, 2001)

Abstract

A modified first-order kinetic law which takes into account defect decay during an ordering process was employed to predict the short-range-order kinetics of a quenched and a quenched-deformed Cu–5 at.% Zn alloy, in conjunction with experiments performed by isothermal calorimetry. The effective activation energy of point defect migration and its temperature dependence strongly suggest the contribution of bound vacancies to the ordering process. An estimate of 91.2 kJ mol^{-1} was made for the activation energy of solute–vacancy migration by applying an effective rate constant, a value in very good agreement with that obtained from previous non-isothermal experiments. The isothermal curves were utilized to determine the ordering energy: $w = -2.90$ kJ mol^{-1}. In conjunction, a parametric study of the defect sink density was performed in order to assess its influence on the calculated isothermal curve profiles.

Keywords: Cu–5 at.% Zn, isothermal calorimetry, kinetics, solute–vacancy complexes

Introduction

Experiments involving short-range-ordering (SRO) kinetics are usually performed after an alloy is quenched from rather high temperatures. Some experiments concentrate on the adjustment of the new equilibrium state of SRO after small and sudden temperature changes [1, 2]. More recent ones are concerned with the influence of cold working [3–5]. All the results are influenced somewhat by the experimental technique and the type of experiment performed. As quenching experiments still provide information about how an excess of point defects frozen in during a quench can affect the ordering kinetics [6–11], the effects of decay during the ordering process need to be considered quantitatively in more detail. Moreover, the presence of solute–vacancy complexes has often been disregarded when effective values of the

* Author for correspondence: Phone: 56–2–678 41 40/678 41 50; Fax: 56–2–671 89 79; E-mail: avarscha@cec.uchile.cl

1418–2874/2001/ $ 5.00

Akadémiai Kiadó, Budapest
Kluwer Academic Publishers, Dordrecht

activation energy of defect migration are measured, and the solute–vacancy binding energy is not negligible.

The present work a) applies a modified first-order kinetic law which describes the SRO kinetics to determine the effective activation energy of point defect migration in Cu–5 at.% Zn, and to estimate the dislocation density in the deformed alloy condition, b) makes an assessment of the activation energy of solute–vacancy pair migration, c) determines the ordering energy from energetic equations by using a suitable plot, and d) utilizes isothermal calorimetry as an experimental tool in order to study SRO kinetics.

Theoretical background

Effective rate constant for SRO

The effective rate at which order is established for a point defect mechanism which includes bound and unbound vacancies is related to the total instantaneous defect concentration, c_t, and to the effective mean rate at which defect atom exchange occurs, i.e. by

$$k_t(T) = c_t(T)\upsilon_t(T) \tag{1}$$

in which

$$\upsilon_t(T) = \upsilon_{0t}\exp\left(-\frac{E}{RT}\right) \tag{2}$$

υ_{0t} being the effective jump frequency constant, E the effective activation energy of total defect migration, T the absolute temperature, and R the universal gas constant.

Here, it will be considered that $c_t=c_u+c_b$, with c_u and c_b equal to the unbound and bound vacancy concentrations. For both diluted and non-diluted alloys, it holds [11] that

$$\frac{c_b}{c_u} = \frac{Zx_t\exp\left(\frac{B}{RT}\right)}{1-(Z+1)x_t + Zx_t\exp\left(\frac{B}{RT}\right)} \tag{3}$$

where Z is the coordination number, x_t is the solute concentration and B is the solute–vacancy binding energy. Thus:

$$\frac{c_b}{c_t} = \frac{Zx_t\exp\left(\frac{B}{RT}\right)}{1-(Z+1)x_t + 2Zx_t\exp\left(\frac{B}{RT}\right)} = \psi_b(T) \tag{4}$$

where $\psi_b(T)$ is here termed the equilibrium transfer function.

As dynamic equilibrium exists during quenching, the concentrations $c_b(T_z)$ and $c_u(T_z)$ at the actual freezing temperature can readily be calculated from $c_b(T_z)=c_t(T_z)\psi_b(T_z)$ and $c_u(T_z)=c_t(T_z)(1-\psi_b(T_z))$. The freezing temperature T_z can be estimated [8] from

$$\frac{E_m}{RT_z}=\ln\left(\frac{RT_z^2}{\phi_q \tau_0 E_m}\right) \tag{5}$$

where $\tau_0=10^{-6}$ s [8] and ϕ_q is the cooling rate.

It should be pointed out that the more mobile unbound vacancies with migration energy E_m determine T_z. Since for this alloy concentration, c_b is close to c_u, separating somewhat with increasing temperature [12], it is safe to take as a first approximation and average activation energy of defect formation $c_t(T_z)=A_s\exp(-E_{ef}/RT_z)$, where $E_{ef}=E_f-B/2$ and $A_s\approx 2$ [8].

For simultaneous unbound and bound vacancy mechanisms, the effective rate constant can be given as

$$\upsilon_t(T)c_t(T)=\upsilon_u(T)c_u(T)+\upsilon_b(T)c_b(T) \tag{6}$$

where $\upsilon_u(T)$ and $\upsilon_b(T)$ are the jump frequencies of unbound and bound vacancies.

The idea involved in Eq. (6) is that the entire population of vacancies, both unbound and bound, is assigned one effective jump frequency, $\upsilon_t(T)=\upsilon_{0m}\exp(-E/RT)$, which is obtained as a weighted sum of simpler jump frequencies describing individual processes. From Eqs (4) and (6), at temperature T, after small transients during the change from the quench-in temperature to the annealing temperature [13]:

$$\upsilon_t=\upsilon_u(1-\psi_b(T))+\upsilon_b\psi_b(T) \tag{7}$$

The simpler jump frequencies are given by $\upsilon_u(T)=\upsilon_{0m}\exp(-E_m/RT)$ and $\upsilon_b(T)=\upsilon_{0m}\exp(-E_c/RT)$, where E_c is the activation energy of migration of bound vacancies. The attempt frequency is considered to be the same for the effective frequency and for unbound and bound vacancies [13]. Its value is given by $\upsilon_{0m}=12\upsilon_0\exp(\Delta S_m/R)$ for f.c.c. alloys, where υ_0 is the Debye frequency and ΔS_m is the activation entropy for free vacancies [10]. Thus:

$$\exp\left(-\frac{E}{RT}\right)=\exp\left(-\frac{E_m}{RT}\right)(1-\psi_b(T))+\exp\left(-\frac{E_c}{RT}\right)\psi_b(T) \tag{8}$$

This relationship will be used later to estimate E_c.

Effective defect decay and short-range-ordering kinetics

Here, we consider that the sink strengths of bound and unbound vacancies are the same and that the total vacancy supersaturation follows a first-order kinetic path, as expected from its elimination at fixed sinks [14]. Defect supersaturation, formally defined as $S=(c_t(T)-c_t^{eq}(T))/(c_t(T_z)-c_t^{eq}(T))$, decays according to

$$\frac{dS}{dt}=-k_d S \tag{9}$$

where $c_t(T)$, c_t^{eq} and $c_t(T_z)$ are the instantaneous, equilibrium and initial defect concentrations, respectively, and $k_d(T)=\rho_t\upsilon_t(T)$ is the rate constant. ρ, the effective sink density, is given by

$$\rho=\rho_d+\rho_g \tag{10}$$

where ρ_d, the sink density for dislocations, can be obtained from

$$\rho_d=\frac{2\pi b^2\delta}{\ln\left(\frac{r_s}{r_c}\right)} \tag{11}$$

with r_s equal to the average distance between dislocations, r_c the capture radius of a dislocation, δ the dislocation density and b the atom jump distance. For grain boundaries, the sink density ρ_g is given by

$$\rho_g=\frac{\lambda}{L^2} \tag{12}$$

where $\lambda=a_0^2/12$ for f.c.c. metals, a_0 is the lattice parameter and L is the grain size. With use of the definition of S, integration of Eq. (11) yields

$$c_t(T)=c_t^{eq}(T)+(c_t(T_z)-c_t^{eq}(T))\exp[-k(T)t] \tag{13}$$

As long as the ordering reaction follows a first-order kinetic law [14, 15], by analogy with non-isothermal experiments [8], the reacted fraction for isothermal conditions, y, can be written as

$$y=1-\exp\left(-\int_0^t k_t(T)dt\right) \tag{14}$$

From Eqs (1) and (13), integration of Eq. (14) leads to

$$y=1-\exp\left\{\frac{k_t(0)-k_t^{eq}(T)}{k_d(T)}[\exp(-k_d(T)t-1)]-k_t^{eq}(T)t\right\} \tag{15}$$

where $k_t(0)$ and $k_t^{eq}(T)$ are the initial and equilibrium rate constants at the annealing temperature, respectively. This equation describes the ordering features considering the parallel evolution of defect supersaturation.

Numerical results and discussion

The preparation details relating to similar alloys can be found elsewhere [9]. One group of specimens were annealed at 973 K, followed by quenching, while another group were quenched from the same temperature and subsequently 40% cold-rolled.

The quench prior deformation was made to achieve a defined reference state of order. A freezing temperature T_z=950 K was calculated by using Eq. (5).

Figure 1 depicts the differential isothermal calorimetric traces for the annealed and quenched alloys at the indicated temperatures. As expected, the higher the annealing temperature, the sharper the curves are, indicating a higher rate of reaction here, characterized by one exothermic peak. Further, the area of the peaks decreases with increasing temperature because a lower equilibrium degree of order is reached, as expected.

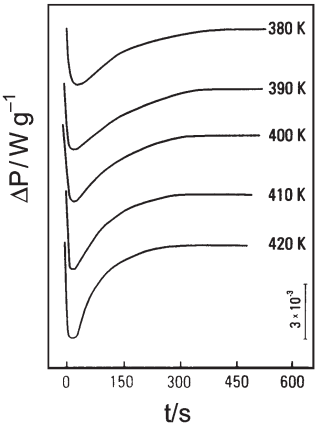

Fig. 1 Isothermal traces at the indicated temperatures for Cu–5 at.% Zn quenched from 973 K

In the following, the effective activation energy of total defect migration will be estimated according to Eq. (15). Before this, the required parameters must be selected. For a typical annealed material, the dislocation density is about $\delta=10^7$ cm^{-2} [8]. For this value, the term $2\pi b^2/\ln(r_s/r_c)$ in Eq. (11), which is relative insensitive to

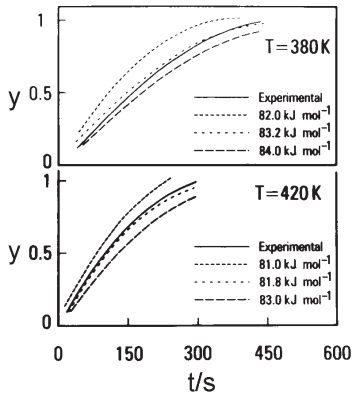

Fig. 2 Reacted fraction *vs*. time curves at the indicated temperatures, with the effective activation energy of defect migration used as an adjusting parameter

the dislocation density for annealed alloys, was $4.4\cdot10^{-16}$ cm^2, and hence $\rho_d=4.4\cdot10^{-9}$. The measured grain size was L=100 μm, a_0=0.36 nm and $\lambda=1.1\cdot10^{-16}$ cm^2; thus from Eq. (12), $\rho_g=1.1\cdot10^{-12}$, which is negligible as compared with ρ_d for this grain size. The effective activation energy of defect formation was taken as E_f–B/2, the activation energy for unbound vacancies being E_f=90.8 kJ mol^{-1} [15] and the solute–vacancy binding energy B=21.8 kJ mol^{-1} [9], and the frequency constant was taken as $\upsilon_{0m}=4.3\cdot10^{14}$ s^{-1} [9]. In order to calculate the freezing temperature, the quench time was measured and estimated as 200 ms, giving a quench rate $\phi_q=3.5\cdot10^3$ K s^{-1}. The activation energy of unbound vacancy migration was obtained as an interpolated value between those for pure copper and Cu–30 at.% Zn [15], giving E_m=80 kJ mol^{-1}. The reacted fraction $y(t)$ is the integral of the curves up to time t divided by the total area under the curve. With the above chosen parameters, two y *vs*. t curves at the extreme chosen indicated temperatures were plotted in Fig. 2. The best fits of the model to the experimental curves were obtained for effective migration energies of 83.2 and 81.8 kJ mol^{-1} at 380 and 420 K, respectively. From similar curves not shown here, values of 82.9, 82.2 and 81.1 kJ mol^{-1} were found at 390, 400 and 410 K, respectively. The larger effective activation energies than that for monovacancies, together with the slight systematic increase at lower temperatures, is consistent with the presence and also with the relative increase in the less mobile bound vacancies with respect to the unbound ones as the temperature decreases. In order to estimate the activation energy of migration of bound vacancies E_c, Eq. (8) can be rewritten as

$$\frac{E_c}{R}\left(\frac{1}{T}\right)=\ln\left[\frac{\psi_b(T)}{\exp\left(-\frac{E}{RT}\right)-\exp\left(-\frac{E_m}{RT}\right)(1-\psi_b(T))}\right] \tag{16}$$

With the right-side term of Eq. (16) designated by $\beta(T)$, a plot of β *vs*. $1/T$ resulted in a straight line, as shown in Fig. 3. The slope of this line, E_c/R, gives

$$E_c=91.2 \text{ kJ mol}^{-1}$$

Such a value is quite reasonable since it lies between E_m and E_m+B, the activation energy for complex dissolution [13, 16]. These results also confirm that in this alloy the bound vacancies are less mobile than the unbound vacancies.

It is also possible to estimate the ordering energy w from isothermal curves at different temperatures in a quenched alloy. In fact, when a quench is performed from T_q=973 K to T=293 K as in the present case, it can be assumed that from T_q to the freezing temperature T_z=950 K, the degree of SRO maintains its dynamic equilibrium value in consequence the enhanced diffusion taking place at these high temperatures. Henceforth, the alloy is at room temperature in a state of order in equilibrium at T_z. If the temperature is subsequently raised to T, it can readily be derived from Eqs (17) and (18) in [17] that the evolved enthalpy is given by

$$\Delta H = -\frac{2x_t^2(1-x_t)^2 Zw^2}{R}\left(\frac{1}{T_z}-\frac{1}{T}\right) \quad (17)$$

Hence, a plot of ΔH values from Fig. 1 *vs*. $(1/T_z - 1/T)$ allows the computation of w from the slope of the resulting straight line. Such a plot is shown in Fig. 4 giving

$$w = -2.90 \text{ kJ mol}^{-1}$$

This value is in very good agreement with the –3.08 kJ mol^{-1} reported in a previous paper [9].

The isothermal traces corresponding to the deformed alloy are shown in Fig. 5 for the same annealing temperatures as those for the annealed material. These temperatures are low enough for recovery by dislocation rearrangement to be absent [18]. Accordingly, if it is taken into account that the heat associated with defect annihilation is more than one order of magnitude less than that involved in the isothermal traces [19], this heat can be associated with SRO degree variations. These curves can be seen to be characterized by one exothermic peak with a slower decay than for the

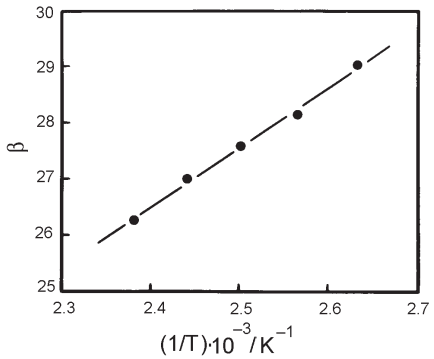

Fig. 3 β *vs*. the reciprocal of the annealing temperature

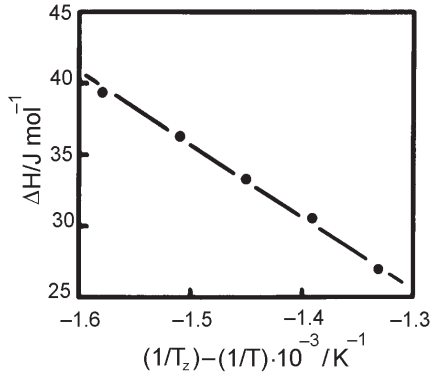

Fig. 4 Reaction enthalpy *vs*. $(1/T_z - 1/T)$, T_z being the freezing temperature and T the temperatures corresponding to the isothermal traces

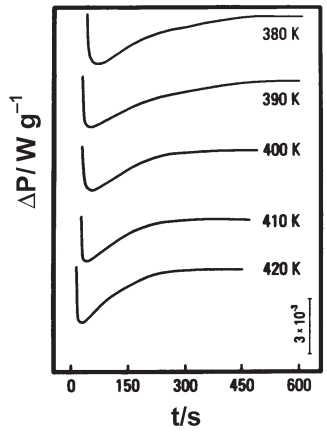

Fig. 5 Isothermal traces at the indicated temperatures for Cu–5 at.% Zn quenched from 973 K and 40% deformed by cold-rolling

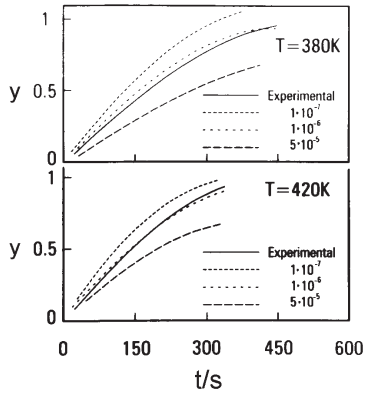

Fig. 6 Reacted fraction *vs*. time curves at the indicated temperatures for the quenched-deformed alloy, with the sink density used as an adjusting parameter

annealed alloy. Further, the heights of the corresponding peaks are smaller. The *y vs*. *t* curves are plotted for 380 and 420 K in Fig. 6, using the corresponding values already obtained for the effective activation energies of defect migration calculated for the annealed alloys with the sink density taken as an adjusting parameter. This assumes as a first approximation that deformation does not alter the concentration ratio of bound to unbound vacancies. For both curves, the best fits are obtained with an average sink density of about $\rho=1.5\cdot10^{-6}$ ($\delta=0.3\cdot10^{10}$ cm^{-2}). This value is in good accord with that to be expected from the metallurgical state of the alloy.

The areas under the isothermal traces for the deformed material were observed to be lower than those for that quenched at each corresponding annealing temperature. Such behaviour may be attributed to the fact that the instantaneous concentration of deformation-induced point defects during the rolling procedure, together with

the presence of point defects arising from quenching, are able to reorder the alloy at room temperature to a higher degree than that after quenching before deformation.

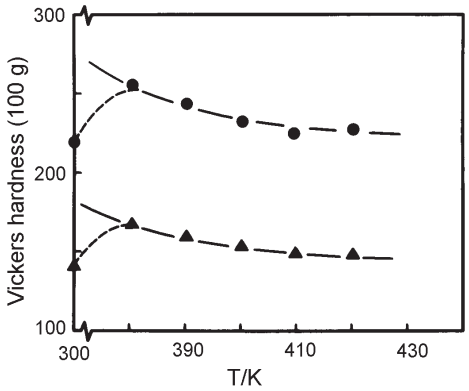

Fig. 7 Vickers hardness *vs*. temperatures corresponding to the isothermal traces after the equilibrium degree of SRO was reached; • – quenched and 40% cold-rolled alloy, ▲– quenched alloy. Room temperature values after quenching before any isothermal treatment are also indicated

Vickers hardness against annealing temperature curves are shown in Fig. 7 after the SRO *y vs. t* plots approach unity. The decrease in hardness observed as the temperature increases in both the annealed and the deformed alloys is a reflection of the equilibrium decrease in SRO at higher temperatures, as may be expected. On the other hand, the constancy of the enthalpy difference between the two alloys means that no recovery takes place in the cold-rolled alloy. On use of the approach in ref. [19] to evaluate energy variations associated with SRO equilibrium changes, the degree of order reached after rolling was calculated to be equivalent to that at equilibrium at 845 K. Additionally, the low stacking fault density expected for this alloy [20] favours non-conservative dislocation motion, which generates increased point defects during deformation processes. This type of motion would be easier for less dissociated dislocations, i.e. for alloys with high stacking fault energies. Because of the high sink density, the surplus point defects partially anneal out very rapidly, thereby contributing less to the ordering process during the isothermal treatment. This fact can explain the lower ordering kinetics exhibited by the cold-rolled material, which probably reaches the equilibrium degree of order with the assistance of thermal point defects.

A family of isothermal traces with the defect sink density taken as a varying parameter are plotted for T=420 K in Fig. 8. This plot predicts that, for $\rho>10^{-5}$, ordering degrees close to that prevailing at equilibrium at T_z are reached since the enthalpy involved in the reaction vanishes. In contrast, for low defect sink densities, the reaction enthalpy becomes insensitive to them, which is the case for an annealed alloy, as may be expected.

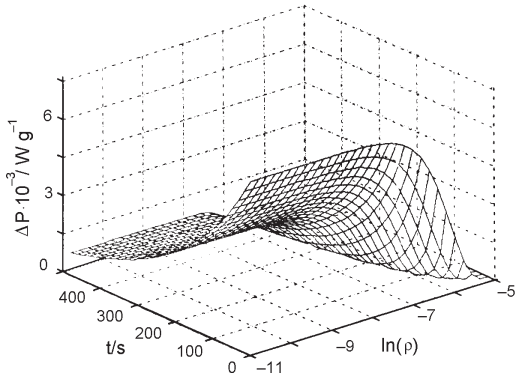

Fig. 8 Three-dimensional plot of isothermal traces at T=420 K, with the sink density ρ taken as the adjusting parameter

Finally, it is worth recalling that in the quenched and deformed material, for the sink density level calculated here, $\rho=1.5\cdot10^{-6}$, and considering the low misfit parameter e_a=0.054 for this alloy system [21], solute segregation to partial dislocations can be disregarded. In fact, with the application of Eqs 2, 20 and 21 in reference [22] and the use of appropriate data for Cu–Zn alloys, the evolved heat due to segregation is found to be 0.55 J mol^{-1}, which is negligible as compared with 46.6 J mol^{-1} for the heat evolved during the ordering process. Specific computations are not shown for the sake of brevity.

Conclusions

The use of a modified first-order kinetic law allows a quite good reproduction of the results of experimental isothermal calorimetric experiments on ordering under both non-deformed and deformed alloy conditions. The effective activation energies of defect migration are consistent with a simultaneous vacancy and solute–vacancy mechanism controlling the ordering process. The estimated solute–vacancy activation energy of migration, 91.2 kJ mol^{-1}, seems a very reasonable value, as also is the ordering energy, estimated as –2.90 kJ mol^{-1}.

* * *

The authors would like to thank the Fondo de Desarrollo Científico y Tecnológico (FONDECYT) for the financial support granted through Project 1980731, and the Instituto de Investigaciones y Ensayes de Materiales (IDIEM), Facultad de Ciencias Físicas y Matemáticas, Universidad de Chile, for the facilities provided for this research.

References

1 M. Migschitz, F. Laugmayr and W. Pfeiler, Mater. Sci. Eng. A, 17 (1994) 217.
2 M. Migschitz, W. Garlipp and W. Pfeiler, Mater. Sci. Eng. A, 214 (1996) 17.

3 M. Spanl, P. Rosenkranz and W. Pfeiler, Mater. Sci. Eng. A, 234 (1997) 541.
4 M. Migschitz and W. Pfeiler, Mater. Sci. Eng. A, 206 (1996) 155.
5 M. Spanl, A. Korner, W. Pfeiler and W. Püschl, Scr. Materialia, 41 (1999) 505.
6 A. Varschavsky and E. Donoso, Mater. Sci. Eng. A, 145 (1991) 95.
7 A. Varschavsky,Thermochim. Acta, 203 (1992) 391.
8 A. Varschavsky and M. Pilleux, Mater. Letts., 17 (1993) 364.
9 E. Donoso and A. Varschavsky, J. Thermal Anal., 45 (1995) 419.
10 A. Varschavsky and E. Donoso, Mater. Sci. Eng. A, 212 (1996) 265.
11 W. Pfeiler, JOM, 52 (2000) 14.
12 D. V. Ragone, Thermodynamics of Materials, Vol. 2, Wiley, 1995, p. 73.
13 A. C. Dasmask and E. J. Dienes, Acta Metall., 12 (1964) 797.
14 W. Pfeiler, Acta Metall., 36 (1988) 2.
15 E. Balanzat and J. Hillairet, P. Phys. F: Metal. Phys., 11 (1981) 1977.
16 A. Varschavsky and E. Donoso, J. Therm. Anal. Cal., (in press).
17 A. van Den Beukel and S. Radelaar, Acta Metall., 31 (1983) 419.
18 L. M. Clarebrough, M. E. Hargreaves and M. H. Loretto, Proc. Roy. Soc., A, 257 (1960) 363.
19 W. P. Pfeiler, P. Meisterle and M. Zehetbauer, Acta Metall., (1984) 1053.
20 L. Delehouzé and A. Deruyttere, Acta Metall., 15 (1967) 727.
21 H. W. King, J. Mater. Sci., 1 (1969) 79.
22 A. Varschavsky and E. Donoso, Mater. Letts., 31 (1997) 239.